Pulse-driven robot: Motion via solitary waves

Bolei Deng[1], Liyuan Chen[1], Donglai Wei[2], Vincent Tournat[3], Katia Bertoldi[1,4]*

The unique properties of nonlinear waves have been recently exploited to enable a wide range of applications, including impact mitigation, asymmetric transmission, switching, and focusing. Here, we demonstrate that the propagation of nonlinear waves can be as well harnessed to make flexible structures crawl. By combining experimental and theoretical methods, we show that such pulse-driven locomotion reaches a maximum efficiency when the initiated pulses are solitons and that our simple machine can move on a wide range of surfaces and even steer. Our study expands the range of possible applications of nonlinear waves and demonstrates that they offer a new platform to make flexible machines to move.

INTRODUCTION

Flexible structures capable of sustaining large deformations are attracting increasing interest not only for their intriguing static response (1–3) but also for their ability to support large amplitude elastic waves. It has been shown that by carefully controlling their geometry, the elastic energy landscape of these highly deformable systems can be engineered to enable the propagation of a variety of nonlinear waves, including vector solitons (4–6), transition waves (7–9), and rarefaction pulses (10, 11). As such, the dynamic behavior of these structures not only displays a very rich physics but also offers new opportunities to manipulate the propagation of mechanical signals, enabling unidirectional propagation (5, 8), mechanical logic (7), wave guiding (12, 13), focusing (14), energy trapping (15), and mitigation (10) and damping of nonlinear periodic vibrations (16).

Here, inspired by both the retrograde peristaltic waves observed in earthworms (Fig. 1A) (17, 18) and the ability of linear elastic waves to generate actuation in ultrasonic motors (19–22), we show that the propagation of nonlinear elastic waves in flexible structures provides opportunities for locomotion. To demonstrate the concept, we focus on a Slinky (Fig. 1B) (23–26)—an iconic stretchable toy that has captivated children and adults all over the world—and use it to realize a pulse-driven robot capable of propelling itself. Our simple machine is built by connecting the Slinky to a pneumatic actuator and using an electromagnet and a plate embedded between the loops to initiate nonlinear pulses that propagate from the front to the back. Notably, we find that the directionality of these pulses enables our simple robot to move forward. Moreover, our results indicate that the efficiency of such pulse-driven locomotion is optimal when the initiated waves are solitons—large amplitude (nonlinear) pulses with stable shape and constant velocity along propagation (4, 5, 7, 8, 10, 27–30). As such, our study expands the range of possible applications of solitary waves and demonstrates that they can also be exploited as simple underlying engines to make flexible machines move.
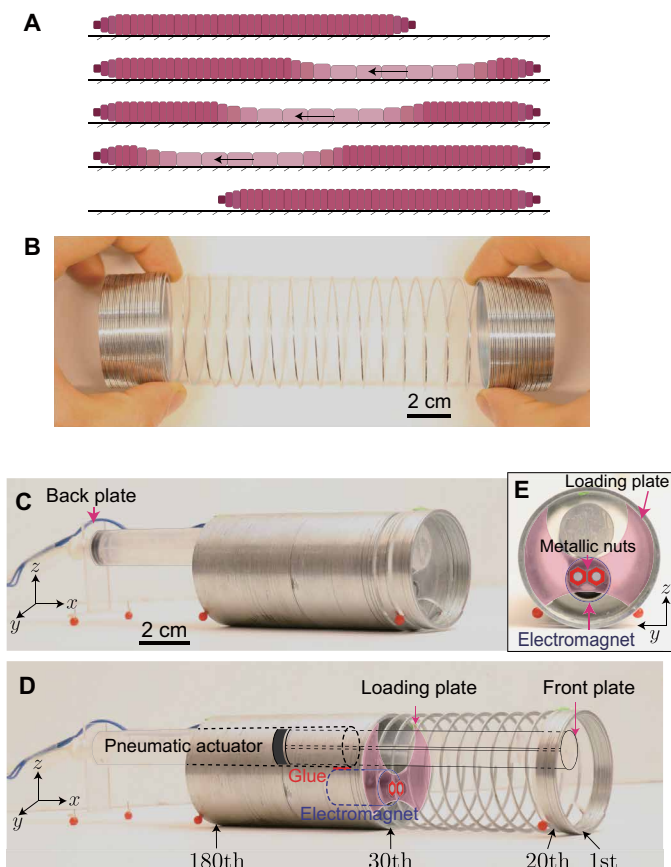
RESULTS

Our Slinky-robot

We consider a metal Slinky with a length of 50 mm, an outer radius of 46.58 mm, and 90 loops, each with mass of $m = 1.01$ g (Fig. 1B

[1]Harvard John A. Paulson School of Engineering and Applied Sciences Harvard University, Cambridge, MA 02138, USA. [2]LAUM, CNRS, Le Mans Université, Av. O. Messiaen, 72085 Le Mans, France. [3]Kavli Institute, Harvard University, Cambridge, MA 02138, USA. [4]Wyss Institute for Biologically Inspired Engineering, Cambridge, MA 02138, USA.
*Corresponding author. Email: bertoldi@seas.harvard.edu

and section S1) and investigate how to exploit its intrinsic flexibility to realize a simple machine capable of rectilinear locomotion. To this end, we connect two Slinkies in series (for a total of 180 loops with length $L = 100$ mm) and implement a simple actuation strategy based on a pneumatic actuator with a stroke of 140 mm (realized using a plastic syringe and a pump), an electromagnet (12V 20N, UXCELL), and three acrylic plates: a front plate inserted between the 20th and 21st loops of the Slinky, a loading plate with an embedded metallic nut fitted between the 30th and 31st loops, and a back plate used to support the tail (Fig. 1, C to E). To construct the robot, we take the pneumatic actuator, connect one of its ends to the front plate, and glue the electromagnet directly on the actuator (Fig. 1D and section S2). When the magnetic field is on, the loading plate remains in contact with the electromagnet, and the 10 loops of the Slinky between the front and loading plates can be stretched and shortened using the pneumatic actuator (Fig. 1E). We test the response of our simple machine by placing it on a smooth and flat surface (Canson Bristol paper) and repeatedly extending the 10 loops to A_{in} (A_{in} being the maximum distance between the loading and front plates; Fig. 2A). We monitor the tests with a high-speed camera (SONY RX100) and extract the displacement of the head, u_h, by tracking the position of the front plate via a superpixel-based method (31).

We start by actuating the Slinky while keeping the electromagnet on. In Fig. 2A, we report snapshots taken during a test, in which we repeatedly extend the front 10 loops to $A_{in} = 100$ mm. Although the head of the robot reaches $u_h^{max} = \max(u_h) = 80$ mm when the actuator is fully extended, because of the symmetric frictional properties it goes back to the initial position at the end of each cycle (Fig. 2B); therefore, no forward motion is achieved (Fig. 2A and movie S1). Next, in an attempt to break symmetry and make our machine crawl, we turn off the magnetic field after stretching the front loops to $A_{in} = 100$ mm. As soon as the electromagnet is turned off, the stretch in the front loops results in the excitation of a wave that propagates backward and reaches the back end of the Slinky (Fig. 2C and movie S1). Note that no reflected wave is observed in the Slinky because of the large energy dissipation upon collisions of the loops. We find that the propagation of this unidirectional pulse results in a nonzero u_h at the end of each cycle—a clear indication that our robot moves forward. Specifically, if we denote with u_h^{cycle} the difference between the displacement of the head at the end and at the beginning of a specific cycle, we find that $u_h^{cycle}/L = 0.32 \pm 0.02$ (green line in Fig. 2B). Therefore, our results indicate that the directionality introduced by the elastic waves can be exploited to make the robot move even in the presence of identical friction coefficients in backward

Fig. 1. Our Slinky-robot. (**A**) Schematic showing the locomotive mechanism of an earthworm based on retrograde peristaltic waves (i.e., waves that propagate in the opposite direction to locomotion). (**B**) Picture of metallic Slinky used in this study. (**C** and **D**) Pictures of our Slinky-robot (C) before and (D) after the pneumatic actuator is elongated. (**E**) Front view of the Slinky-robot showing the electromagnet. Note that several red plastic spheres are glued on to the Slinky to prevent it from rolling. Photo credit: Bolei Deng, Harvard University.

and forward directions. Furthermore, we also find that the phenomenon is robust as the robot behaves almost identically during various cycles (Fig. 2B).

Although our results indicate that the propagation of elastic pulses can be exploited to make our flexible machine crawl, they also reveal that the conditions used in our experiments are not optimal because there is noticeable backsliding immediately after the electromagnet is turned off. Specifically, if we focus on the first cycle, we find that u_h suddenly drops from $u_h^{max} = 0.8L$ to about $u_h^{cycle} = 0.32L$ (Fig. 2B). To limit such backsliding, we increase the mass at the head, m_h. In Fig. 2D, we report the average value of u_h^{cycle} over three cycles as a function of m_h/m_{tot} (m_{tot} being the total mass of the Slinky). While for the robot considered in Fig. 2C (for which $m_h/m_{tot} = 0.23$) $u_h^{cycle} = 0.32L$, we find that for $0.26 < m_h/m_{tot} < 0.39$ u_h^{cycle} increases to ~0.45L. However, if $m_h/m_{tot} > 0.4$, u_h^{cycle} then suddenly drops as the weight prevents the head to move forward when the pneumatic actuator is extended (movie S2).

Having identified an optimal range for m_h, we choose $m_h/m_{tot} = 0.32$ (resulting in $m_h = 78$ g and $m_{tot} = 246$ g) and investigate the effect of A_{in} on the ability of our robot to crawl (Fig. 2E). As expected, we find that u_h^{cycle} monotonically increases with A_{in}. However,

more insight into the role of A_{in} can be gained by calculating the efficiency η of such pulse-driven locomotion

$$\eta = \frac{W_{req}}{W_{in}} \quad (1)$$

where W_{req} denotes the work required for the robot to move on the substrate against friction and W_{in} is the work supplied to initiate the pulse. Specifically, if we denote with μ the friction coefficient between the Slinky and the substrate

$$W_{req} = \mu\, m_{tot}\, g\, u_h^{cycle} \quad (2)$$

and

$$W_{in} = \mu\, m_h g\, u_h^{max} + n_a \int_0^{\frac{A_{in}}{n_a}} F(\Delta u)\, d\Delta u \quad (3)$$

where g is the gravitational constant, n_a is the number of loops between the loading and front plates, and F denotes the force required to stretch one loop of the Slinky by Δu. Note that the first term of Eq. 3 stands for the work done to move the head of the Slinky, while the second one represents the elastic energy stored in the front n_a loops, which is eventually carried by the excited pulse. For the tests considered in Fig. 2, $n_a = 10$ and we measure μ = 0.17. Moreover, we obtain the F-Δu relation by conducting a quasistatic uniaxial tension test on a portion of the Slinky (see Fig. 2F and section S1 for details). In Fig. 2G, we plot the evolution of η as a function of A_{in} obtained using Eqs. 1 to 3. Notably, we find that the efficiency of our machine is maximum for $A_{in} = 100$ mm. While in Fig. 2G we focus on a robot in which 10 loops are prestretched, this result persists also when we vary n_a. In particular, as shown in Fig. 2H, we find that for a wide range of n_a, the efficiency is maximum at $A_{in} = 100$ mm. However, such maximum decreases if $n_a < 7$ or $n_a > 16$. For large values of n_a, the energy carried by the excited pulses is small (see fig. S7) and not enough to make them propagate in the presence of friction (see movie S3). Differently, when n_a is too small, the energy carried by the pulses is large, making the pulse to reach the back of the Slinky (see movie S3). At this point, u_h^{cycle} saturates (see fig. S7) and the efficiency drops because part of the energy carried by the pulse is lost through collisions between the loops.

Propagation of nonlinear waves

To understand why the efficiency of our robot is maximum for $A_{in} = 100$ mm, we carefully investigate the propagation of large-amplitude pulses through the Slinky. In these tests, we focus on a single Slinky (with $N = 90$ loops) and monitor the position of green markers located at every other loop. Moreover, to minimize the effect of friction, we lift the Slinky from the substrate and use a plastic rod to support it (Fig. 3A). As in the tests conducted on our Slinky-robot, we find that by prestretching 10 loops near the front and turning off the magnetic electromagnet, we can initiate elastic waves that propagate toward the back (Fig. 3B). Furthermore, these tests enable us to get deeper insights into the propagation of the pulses because we monitor the displacement of each individual loop (movie S4). In particular, two important features emerge from these tests. First, we find that the backward-propagating waves move the center of mass of the Slinky forward (Fig. 3C)—an observation that further explains how the pulses make our Slinky-robot move. Second, we find that for $A_{in} = 100$ mm, the excited waves propagate while maintaining
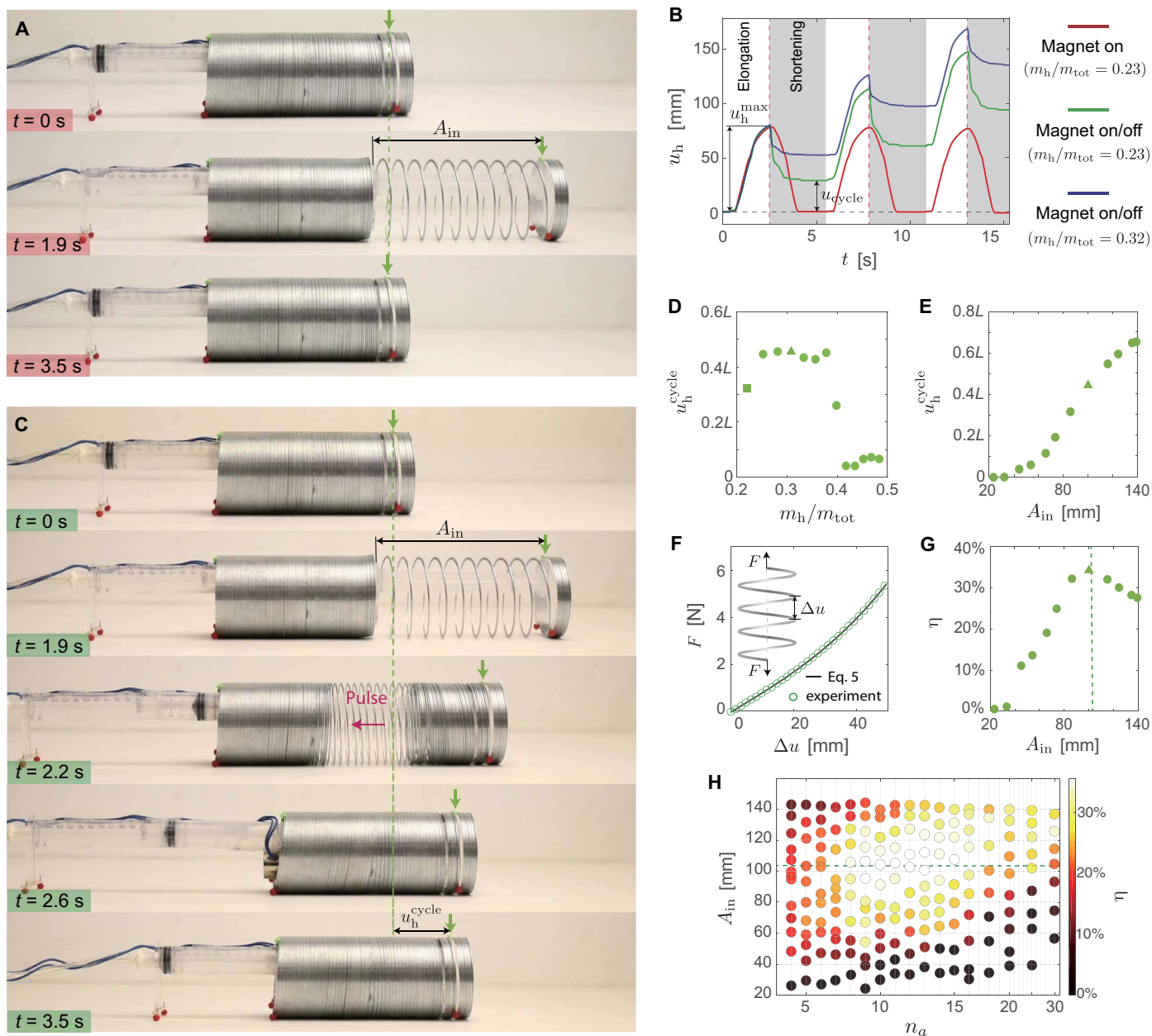
**Fig. 2. Performance of the Slinky-robot.** (**A**) Snapshots taken during a test in which we extend the front 10 loops to A_{in} = 100 mm while keeping the electromagnet on. (**B**) Displacement of the head during three cycles for tests in which (i) m_h/m_{tot} = 0.23 and we keep the electromagnet on (red line), (ii) m_h/m_{tot} = 0.23 and we turn off the electromagnet after stretching (green line), and (iii) m_h/m_{tot} = 0.32 and we turn off the electromagnet after stretching (blue line). (**C**) Snapshots taken during a test in which A_{in} = 100 mm and we turn the electromagnet off after stretching the front loops. (**D**) Evolution of u_h^{cycle} as a function of m_h/m_{tot} for tests in which A_{in} = 100 mm. The square and triangular markers correspond to m_h/m_{tot} = 0.23 and 0.32, respectively. (**E**) Evolution of u_h^{cycle} as a function of A_{in} for tests in which m_h/m_{tot} = 0.32. The triangular marker corresponds to A_{in} = 100 mm. (**F**) Static response of the Slinky as measured in a uniaxial test. (**G**) Evolution of η as a function of A_{in} for tests in which m_h/m_{tot} = 0.32. The triangular markers correspond to A_{in} = 100 mm. The green dashed line corresponds to the amplitude of the supported soliton, A_s. (**H**) Evolution of η as a function of n_a and A_{in} for tests in which m_h/m_{tot} = 0.32. Photo credit: Bolei Deng, Harvard University.

their shape at a constant velocity of 279 loop/s, with only slight acceleration near the end due to boundary effects (Fig. 3D). This suggests that the Slinky supports the propagation of large-amplitude solitary waves. To further confirm this observation, we calculate the cross-correlation of the velocity signals measured at the 10th and 80th loops (Fig. 3E). We find that the cross-correlation is maximum

and approaches unity for A_{in} = 100 mm (movie S4), the same amplitude that maximizes the efficiency of our Slinky-robot (see Fig. 2G).

To provide deeper insight into these experimental results, we developed a mathematical model based on a one-dimensional array of concentrated masses m connected by nonlinear springs, which represent the mass and elasticity of an individual loop, respectively
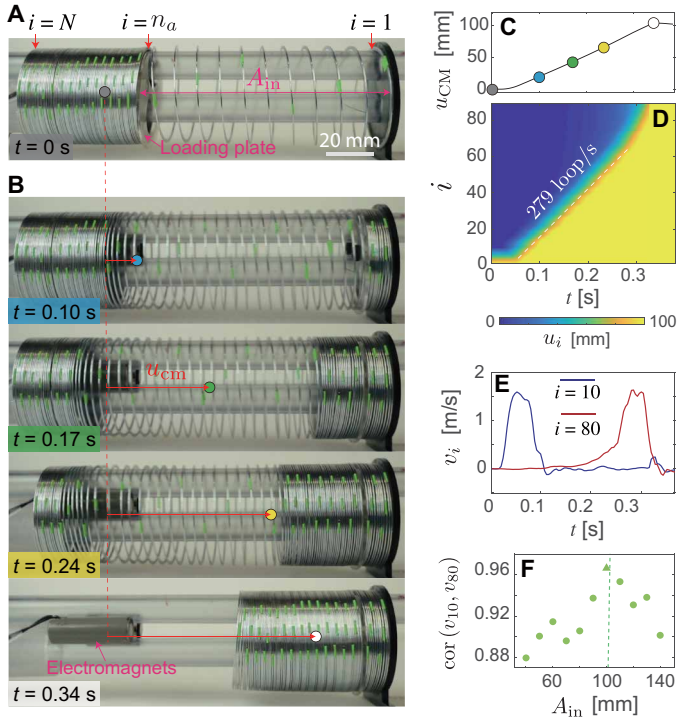
Fig. 3. Wave propagation in the Slinky. (**A**) Experimental setup used to test the propagation of pulses in the metallic Slinky. At $t = 0$ s, $n_a = 10$ loops between the loading plate and the front of the Slinky are stretched to $A_{in} = 100$ mm. (**B**) Snapshots of the propagation of the pulse in the Slinky at $t = 0.10$, 0.17, 0.24, and 0.34 s. The circular markers indicate the positions of the center of mass of the Slinky. (**C**) Displacement of the center of mass of the Slinky, u_{CM}, as a function of time. Circular markers correspond to the time points considered in (A) and (B). (**D**) Spatiotemporal displacement diagram of the propagating pulse. (**E**) Velocity signals measured at the 10th and 80th loops. (**F**) Evolution of the cross-correlation of $v_{10}(t)$ and $v_{80}(t)$ as a function of the input amplitude A_{in}. The triangular marker corresponds to $A_{in} = 100$ mm. The green dashed line corresponds to the amplitude of the supported soliton, A_s, predicted by Eq. 10. Photo credit: Bolei Deng, Harvard University.

(Fig. 4A). The governing equations for such discrete system can be written as

$$m \frac{\partial^2 u_i}{\partial t^2} = F(u_{i+1} - u_i) - F(u_i - u_{i-1}) \tag{4}$$

where u_i represents the displacement of ith mass and $F(u_{i+1} - u_i)$ denotes the force in the spring connecting the ith and $(i + 1)$th masses. For the Slinky considered in this study, $m = 1.01$ g and the elastic response of an individual loop can be nicely fitted by

$$F(u_{i+1} - u_i) = k [(u_{i+1} - u_i) + \alpha (u_{i+1} - u_i)^3] \tag{5}$$

with a stiffness constant $k = 79.2$ N/m and a cubic nonlinearity parameter $\alpha = 155.1$ m^{-2} (see Fig. 2F and section S3 for details). Note that Eq. 5 only captures the response of the Slinky under tension (i.e., $u_{i+1} - u_i \geq 0$) and therefore limits us to investigate rarefaction wave solutions.

Next, because in our experiments the wavelength of the propagating waves is much wider than a single loop, we take the continuum limit of Eq. 4 and retain derivatives up to fourth order to obtain the continuum governing equation
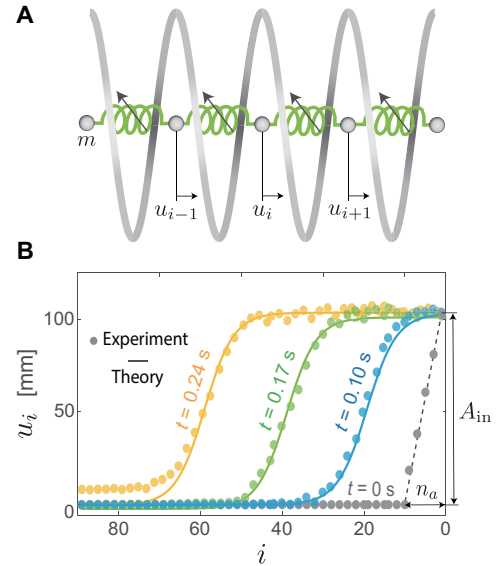
Fig. 4. Mathematical model. (**A**) Schematic of our model. Each nonlinear spring represents the elastic response of an individual loop, whereas each concentrated mass represents its mass. (**B**) Spatial displacement profiles at $t = 0$, 0.10, 0.17, and 0.24 s as measured in our experiments (circular markers) and predicted by our analytical solution given by Eq. 7 (solid lines).

$$\frac{1}{c_0^2} \frac{\partial^2 u}{\partial t^2} = \frac{\partial^2 u}{\partial \xi^2} + \frac{1}{12} \frac{\partial^4 u}{\partial \xi^4} + \alpha \frac{\partial}{\partial \xi} \left(\frac{\partial u}{\partial \xi} \right)^3 \tag{6}$$

where $u(\xi, t)$ is a continuous function that interpolates $u_i(t)$, i.e., $u(\xi = i, t) = u_i(t)$, ξ denotes the loop number, and $c_0 = \sqrt{k/m} = 280.0$ m/s is the velocity of linear waves in the long-wavelength regime. Equation 6 has been shown to be equivalent to the generalized Boussinesq equation and admits an analytical solution in the form of a rarefaction solitary wave (*32*)

$$u = -\sqrt{\frac{2}{3\alpha}} \arctan \left[\tanh \left(\frac{\xi - \xi_0 - c t}{W} \right) \right] + \frac{\pi}{4} \sqrt{\frac{2}{3\alpha}} \tag{7}$$

with

$$W = \sqrt{\frac{1}{3(c^2/c_0^2 - 1)}} \tag{8}$$

where ξ_0 identifies the position of the wave at $t = 0$ and c and W are the velocity and the characteristic width of the pulse, respectively. Because solitary waves propagate maintaining their shape, we require the maximum extension in the Slinky [i.e., max $(\partial u/\partial \xi)$] to be equal to that imposed to the 10 loops before turning off the electromagnets (i.e., A_{in/n_a})

$$\frac{A_{in}}{n_a} = \max \left(\frac{\partial u}{\partial \xi} \right) = \sqrt{\frac{2}{\alpha} \left(\frac{c^2}{c_0^2} - 1 \right)} \tag{9}$$

and in this way obtain a relation between propagation velocity c and the applied input A_{in}. Last, the amplitude of the supported soliton can be calculated as

$$A_s = u(\xi \to \infty) - u(\xi \to -\infty) = \frac{\pi}{\sqrt{6\alpha}} \tag{10}$$
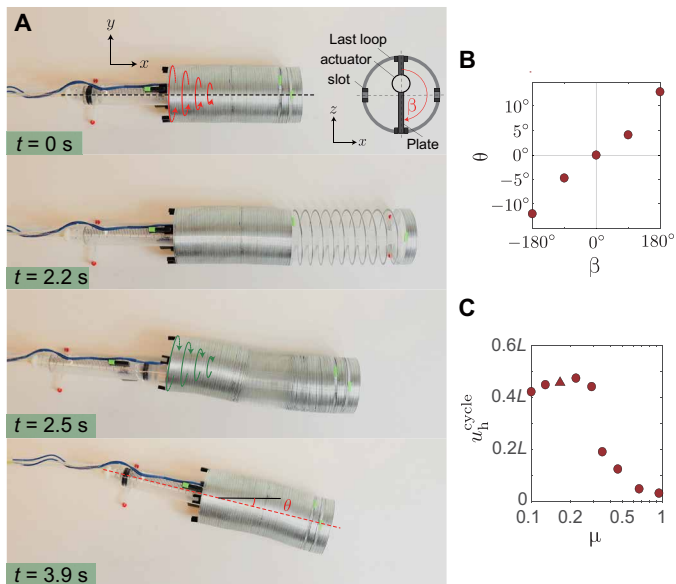
Fig. 5. Steering and moving over different surfaces. (**A**) Snapshots taken during a test in which we twist the last loop by β = 180° before initiating the wave. The Slinky-robot steers by an angle θ = 13° when the pulse reaches its tail. (**B**) Evolution of the steering angle θ as a function of the applied twist β. (**C**) Evolution of u_h^{cycle} as a function of the friction coefficient between the Slinky and the substrate, μ. The triangular marker corresponds to Bristol paper—the substrate considered in Fig. 2. Photo credit: Bolei Deng, Harvard University.

and is found to be an intrinsic property of the Slinky, because it only depends on α (i.e., on the strength of the nonlinear term in its static force-displacement response; see Eq. 5). For the Slinky considered in this study, using Eqs. 8 to 10, we obtain $A_s = 103$ mm, $c = 282.2$ loop/s, and $W = 4.62$ loop—values that match extremely well with the experimental results (Fig. 4B). Note that the model also confirms the experimental observations reported in Fig. 3, as it predicts that only pulses with amplitude $A_{in} \sim A_s = 103$ mm propagate in solitary fashion through the Slinky. Last, our analysis reveals that the efficiency of the Slinky-robot is maximum when the initiated waves are solitons (i.e., when $A_{in} = A_s$; see green dashed lines in Fig. 2, G and H). The nondispersive nature and compactness of solitary pulses make them extremely efficient in transferring the energy provided by the pneumatic actuator to motion, ultimately resulting in the most efficient pulse-driven locomotion.

DISCUSSION

To summarize, we have shown that backward propagating solitons can be harnessed to efficiently make a Slinky-robot move forward. Although limbless organisms have recently inspired the design of a variety of robots (33–40), to the best of our knowledge, this is first robotic system that exploits elastic pulses to move. It is also worth noting that the principles presented in this study are different from those used by ultrasonic motors (19). Our Slinky-robot is flexible and uses nonlinear pulse waves to change the position of the center of mass. By contrast, ultrasonic motors are powered by linear sinusoidal waves, induce local microscopic displacements (eventually adding up over many periods to produce a large motion), and modulate friction by exerting an oscillating normal force between stiff surfaces.

It is important to point out that, while in this study we have focused on rectilinear forward crawling, the flexibility of the Slinky can be exploited to expand the range of achievable motions. For example, we can make the robot steer by twisting the last loop at the back of the robot by an angle β before initiating the wave (Fig. 5A and movie S5) and easily control the steering angle θ by tuning both the direction and magnitude of β (Fig. 5B).

We also want to emphasize that our robot can move over a broad range of surfaces. To demonstrate this point, in Fig. 5C, we report u_h^{cycle} recorded when our Slinky-robot (with $m_h/m_{tot} = 0.32$ and $A_{in} = 100$ mm) moves on surfaces characterized by a broad range of roughness (so that μ ∈ [0.1,1]). Notably, we find that for a μ < 0.3, u_h^{cycle} remains almost constant ($u_h^{cycle} \sim 0.45L$). For larger values of μ, the frictional forces prevent propagation of the pulses and u_h^{cycle} drops significantly—an additional demonstration of the important role played by the wave propagation in achieving locomotion (movie S6).

Last, while in this study we have used a Slinky to realize such pulse-driven locomotion, the principles are general and can be expanded to a broad range of stretchable systems across scales, opening avenues even for microscale crawlers suitable for medical applications.

MATERIALS AND METHODS

The basic properties of the metallic Slinky are provided in section S1. Details on fabrication, testing, and additional results of the Slinky-robot are described in section S2. Details on the experiments conducted to characterize the propagation of nonlinear waves are presented in section S3. Details on the model established to characterize the propagation of nonlinear waves are presented in section S4.

SUPPLEMENTARY MATERIALS

Supplementary material for this article is available at http://advances.sciencemag.org/cgi/content/full/6/18/eaaz1166/DC1

REFERENCES AND NOTES

1. P. M. Reis, A perspective on the revival of structural (in) stability with novel opportunities for function: From buckliphobia to buckliphilia. *J. Appl. Mech.* **82**, 111001 (2015).
2. K. Bertoldi, V. Vitelli, J. Christensen, M. van Hecke, Flexible mechanical metamaterials. *Nat. Rev. Mater.* **2**, 17066 (2017).
3. D. P. Holmes, Elasticity and stability of shape-shifting structures. *Curr. Opin. Colloid Interface Sci.* **40**, 118–137 (2019).
4. B. Deng, J. Raney, V. Tournat, K. Bertoldi, Elastic vector solitons in soft architected materials. *Phys. Rev. Lett.* **118**, 204102 (2017).
5. B. Deng, P. Wang, Q. He, V. Tournat, K. Bertoldi, Metamaterials with amplitude gaps for elastic solitons. *Nat. Commun.* **9**, 3410 (2018).
6. B. Deng, V. Tournat, K. Bertoldi, Effect of predeformation on the propagation of vector solitons in flexible mechanical metamaterials. *Phys. Rev. E* **98**, 053001 (2018).
7. J. R. Raney, N. Nadkarni, C. Daraio, D. M. Kochmann, J. A. Lewis, K. Bertoldi, Stable propagation of mechanical signals in soft media using stored elastic energy. *Proc. Natl. Acad. Sci. U.S.A.* **113**, 9722–9727 (2016).
8. N. Nadkarni, A. F. Arrieta, C. Chong, D. M. Kochmann, C. Daraio, Unidirectional transition waves in bistable lattices. *Phys. Rev. Lett.* **116**, 244501 (2016).
9. B. Deng, P. Wang, V. Tournat, K. Bertoldi, Nonlinear transition waves in free-standing bistable chains. *J. Mech. Phys. Solids* **136**, 103661 (2019).
10. H. Yasuda, Y. Miyazawa, E. G. Charalampidis, C. Chong, P. G. Kevrekidis, J. Yang, Origami-based impact mitigation via rarefaction solitary wave creation. *Sci. Adv.* **5**, eaau2835 (2019).
11. B. Deng, Y. Zhang, Q. He, V. Tournat, P. Wang, K. Bertoldi, Propagation of elastic solitons in chains of pre-deformed beams. *New J. Phys.* **21**, 073008 (2019).
12. J. Vila, G. H. Paulino, M. Ruzzene, Role of nonlinearities in topological protection: Testing magnetically coupled fidget spinners. *Phys. Rev. B* **99**, 125116 (2019).
13. Y. Xia, M. Ruzzene, A. Erturk, Dramatic bandwidth enhancement in nonlinear metastructures via bistable attachments. *Appl. Phys. Lett.* **114**, 093501 (2019).

14. B. Deng, C. Mo, V. Tournat, K. Bertoldi, J. R. Raney, Focusing and mode separation of elastic vector solitons in a 2D soft mechanical metamaterial. *Phys. Rev. Lett.* **123**, 024101 (2019).

15. W. Jiao, S. Gonella, Intermodal and subwavelength energy trapping in nonlinear metamaterial waveguides. *Phys. Rev. Appl.* **10**, 024006 (2018).

16. D. M. J. Dykstra, J. Busink, B. Ennis, C. Coulais, Viscoelastic snapping metamaterials. *J. Appl. Mech.* **86**, 111012 (2019).

17. W. B. Yapp, B. I. Roots, Locomotion of worms. *Nature* **177**, 614–616 (1956).

18. K. J. Quillin, Kinematic scaling of locomotion by hydrostatic animals: Ontogeny of peristaltic crawling by the earthworm lumbricus terrestris. *J. Exp. Biol.* **202**, 661–674 (1999).

19. S. Ueha, Y. Tomikawa, M. Kurosawa, N. Nakamura, *Ultrasonic Motors: Theory and Applications* (Clarendon Press, 1993).

20. T. Sashida, T. Kenjo, *An Introduction to Ultrasonic Motors* (Oxford Univ. Press, 1993).

21. H. Imabayashi, T. Fujimura, T. Funakubo, Ultrasonic motor. US Patent 5,357,164 (1994).

22. N. W. Hagood, A. J. McFarland, Modeling of a piezoelectric rotary ultrasonic motor. *IEEE Trans. Ultrason. Ferroelectr. Freq. Control* **42**, 210–224 (1995).

23. D. P. Holmes, A. D. Borum, B. F. Moore III, R. H. Plaut, D. A. Dillard, Equilibria and instabilities of a slinky: Discrete model. *Int. J. Non-Lin. Mech.* **65**, 236–244 (2014).

24. J. M. Bowen, Slinky oscillations and the notion of effective mass. *Am. J. Phys.* **50**, 1145–1148 (1982).

25. A.-P. Hu, A simple model of a slinky walking down stairs. *Am. J. Phys.* **78**, 35–39 (2010).

26. M. S. Longuet-Higgins, On Slinky: The dynamics of a loose, heavy spring. *Math. Proc. Camb. Philos. Soc.* **50**, 347–351 (1954).

27. M. Remoissenet, *Waves Called Solitons* (Springer-Verlag Berlin Heidelberg, 1999).

28. T. Dauxois, M. Peyrard, *Physics of Solitons* (Cambridge Univ. Press, 2006).

29. R. Zaera, J. Vila, J. Fernandez-Saez, M. Ruzzene, Propagation of solitons in a two-dimensional nonlinear square lattice. *Int. J. Non-Lin. Mech.* **106**, 188–204 (2018).

30. M. I. Hussein, M. J. Leamy, M. Ruzzene, Dynamics of phononic materials and structures: Historical origins, recent progress, and future outlook. *Appl. Mech. Rev.* **66**, 040802 (2014).

31. J. Chang, D. Wei, J. W. Fisher III, A video representation using temporal superpixels, in *2013 IEEE Conference on Computer Vision and Pattern Recognition* (IEEE, 2013), pp. 2051–2058.

32. S. N. Pnevraatikos, Solitons in nonlinear atomic chains. *North-Holland Math. Stud.* **103**, 397–437 (1985).

33. D. Rus, M. T. Tolley, Design, fabrication and control of soft robots. *Nature* **521**, 467–475 (2015).

34. A. Rafsanjani, Y. Zhang, B. Liu, S. M. Rubinstein, K. Bertoldi, Kirigami skins make a simple soft actuator crawl. *Sci. Robot.* **3**, eaar7555 (2018).

35. C. D. Onal, D. Rus, Autonomous undulatory serpentine locomotion utilizing body dynamics of a fluidic soft robot. *Bioinspir. Biomim.* **8**, 026003 (2013).

36. S. Seok, C. D. Onal, K.-J. Cho, R. J. Wood, D. Rus, S. Kim, Meshworm: A peristaltic soft robot with antagonistic nickel titanium coil actuators. *IEEE/ASME Trans. Mechatron.* **18**, 1485–1497 (2013).

37. K. Jung, J. C. Koo, J. D. Nam, Y. K. Lee, H. R. Choi, Artificial annelid robot driven by soft actuators. *Bioinspir. Biomim.* **2**, S42–S49 (2007).

38. A. B. Slatkin, J. Burdick, W. Grundfest, The development of a robotic endoscope, in *Proceedings of the 1995 IEEE/RSJ International Conference on Intelligent Robots and Systems. Human Robot Interaction and Cooperative Robots* (IEEE, 1995), vol. 2, pp. 162–171.

39. E. V. Mangan, D. A. Kingsley, R. D. Quinn, H. J. Chiel, Development of a peristaltic endoscope, in *Proceedings of the 2002 IEEE International Conference on Robotics and Automation (Cat. No. 02CH37292)* (IEEE, 2002), vol. 1, pp. 347–352.

40. J. Aguilar, T. Zhang, F. Qian, M. Kingsbury, B. McInroe, N. Mazouchova, C. Li, R. Maladen, C. Gong, M. Travers, R. L. Hatton, H. Choset, P. B. Umbanhowar, D. I. Goldman, A review on locomotion robophysics: The study of movement at the intersection of robotics, soft matter and dynamical systems. *Rep. Prog. Phys.* **79**, 110001 (2016).